arXiv:1701.03715v1 [cond-mat.mtrl-sci] 13 Jan 2017

The anisotropic ultrahigh hole mobility in strain-engineering two-dimensional penta-SiC_2

Yuanfeng Xu[1], Zeyu Ning[1], Hao Zhang[1,3,*], Gang Ni[1], Hezhu Shao[2], Bo Peng[1], Xiangchao Zhang[1], Xiaoying He[1], Yongyuan Zhu[3] and Heyuan Zhu[1]

[1]*Department of Optical Science and Engineering and Key Laboratory of Micro and Nano Photonic Structures (Ministry of Education), Fudan University, Shanghai 200433, China*

[2]*Ningbo Institute of Materials Technology and Engineering, Chinese Academy of Sciences, Ningbo 315201, China*

[3]*Nanjing University, National Laboratory of Solid State Microstructure, Nanjing 210093, China*

Using the first-principles calculations based on density functional theory, we systematically investigate the strain-engineering (tensile and compressive strain) electronic, mechanical and transport properties of monolayer penta-SiC_2. By applying an in-plane tensile or compressive strain, it is easy to modulate the electronic band structure of monolayer penta-SiC_2, which subsequently changes the effective mass of carriers. Furthermore, the obtained electronic properties are predicted to change from indirectly semiconducting to metallic. More interestingly, at room temperature, uniaxial strain can enhance the hole mobility of penta-SiC_2 along a particular direction by almost three order in magnitude, *i.e.* from 2.59 $\times 10^3 cm^2/Vs$ to 1.14 $\times 10^6 cm^2/Vs$ (larger than the carrier mobility of graphene, 3.5 $\times 10^5 cm^2/Vs$), with little influence on the electron mobility. The high carrier mobility of monolayer penta-SiC_2 may lead to many potential applications in high-performance electronic and optoelectronic devices.

I. INTRODUCTION

Two-dimensional (2D) materials have attracted great attention in the fields of nanoscale materials and nanotechnology since the experimental realization of graphene[1–3], which possesses remarkable mechanical, electronic and optical properties[4–6] possibly leading to many novel applications in microelectronic and optoelectronic devices. A large number of graphene-like structures and other layered structures with different chemical compositions and different crystal structures have been proposed and synthesised since then. Recently, Zhang *et al.*[7], predicted a new 2D material composed of carbon pentagons, *i.e*. penta-graphene, with mixed sp^2/sp^3 orbital hybridization, which is dynamically and mechanically stable, and can withstand temperatures as high as 1000 K. Monolayer penta-graphene possesses unusual negative Poisson's ratio, ultrahigh ideal strength outperforming graphene and other interesting electronic properties[7,8], which make it a potential candidate for wide applications in the optoelectronics and photovoltaics devices.

Many efforts have been devoted on the discovery of new 2D materials with penta strcuture since the successful prediction of penta-graphene. The silicon counterpart of the penta structure was proposed as well, although it is dynamically instable in the monolayer form[9]. Recently, a novel pentagonal structure composed of carbon and silicon atoms in a sp^2d^2 hybridization, *i.e*. pentagonal silicon dicarbide (penta-SiC_2)[10], is proposed and further confirmed to be dynamically stable and exhibits enhanced similar electronic property compared to penta-graphene.

During the processes of experimental realization of 2D materials, mismatch between 2D material and substrate often results in the formation of crystal distortion due to strain or stress modulation. Experimental measurements of physical properties of 2D materials could be different from those with perfect structures. Therefore it is necessary to investigate the strain-dependence properties of 2D materials comparing experimental results. In addition, strain-engineering (external strain and stress) is an effective way to modulate the electronic, mechanical, optical properties and transport of 2D materials[11–14]. It has been reported that strain engineering can be used to modulate the electronic properties of MoS_2[15], black phosphorene[16],TiS_3[17] and ReS_2[13]. The strain-engineering method was proved to be effective in increasing the band gap of pengta-SiC_2[10] as well. However, further investigation on the carrier mobility of monolayer penta-SiC_2 under various strain has not been addressed.

In this work, we systematically investigate electronic, mechanical and transport properties of monolayer penta-SiC_2 under tensile and compressive strain by using first-principles calculations.

We find that under in-plane uniaxial strain, penta-SiC_2 remains an indirect semiconductor until 22%, however, the uniaxial compressive strain can easily converted it from semiconducting into metallic beyond −15%. When applying a biaxial strain, penta-SiC_2 can change from semiconductor to metallic material under relatively low compressive strain of −8%. In general, the electronic band structure of penta-SiC_2 is sensitive to tensile and compressive strain. Moreover, we have quantitatively demonstrated that the carrier mobility can be enhanced from 2.59 $\times 10^3 cm^2/Vs$ to 1.14 $\times 10^6 cm^2/Vs$ by applying a uniaxial compressive strain.

II. METHOD AND COMPUTATIONAL DETAILS

The calculations are performed using the Vienna *ab-initio* simulation package (VASP) based on density functional theory[18]. The exchange-correlation energy is described by the generalized gradient approximation (GGA) using the Perdew-Burke-Ernzerhof (PBE) functional. The calculationa are carried out by using the projector-augmented-wave pseudo potential method with a plane wave basis set with a kinetic energy cutoff of 500 eV. When optimizing atomic positions, the energy convergence value between two consecutive steps is chosen as 10^{-5} eV and the maximum Hellmann-Feynman force acting on each atom is 10^{-3} eV/Å. The Monkhorst-Pack scheme is performed for the Brillouin zone integration with k-point meshes of 13×13×1 and 21×21×1 for geometry optimization and self-consistent electronic structure calculations, respectively. To verify the results of the PBE calculations, the electronic structure of penta-SiC_2 with zero strain is calculated using hybrid Heyd-Scuseria-Ernzerhof (HSE06) functional[19]. HSE06 improves the precision of band gap by reducing the localization and delocalization errors of PBE and HF functionals. The mixing ratio used in the HSE06 is 25% for short-range Hartree-Fock exchange. The screening parameter u is set to be 0.4 $Å^{-1}$.

III. RESULTS AND DISCUSSION

A. Electronic band structure of penta-SiC_2

The top and side views of the fully optimized structure of penta-SiC_2 are shown in Fig. 1(a) and (b), respectively. The unit cell (the red dashed rectangle) contains two silicon atoms and four carbon atoms. The optimized penta-SiC_2 has a tetragonal crystal structure with the space group of $p\bar{4}2_1m$. As shown in Fig. 1(a) and (b), all pentagons contain four equivalent Si-C bonds and one

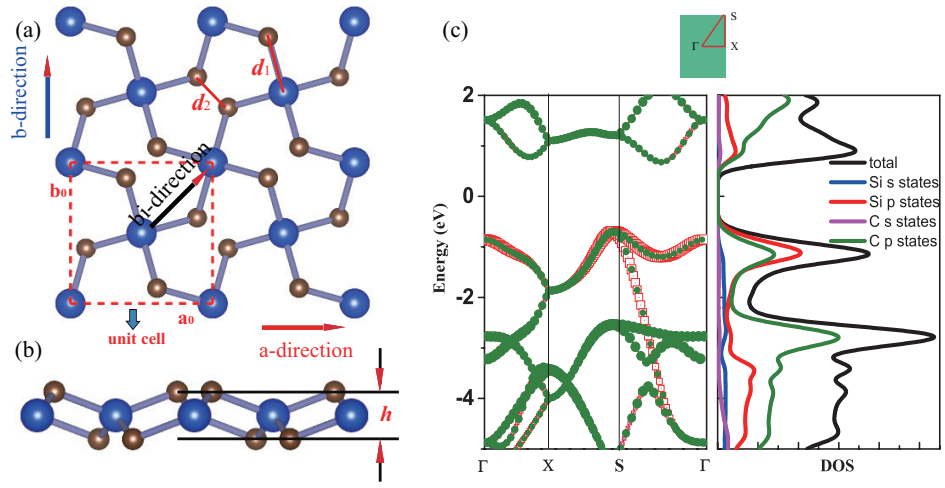

FIG. 1. (a) Top view (b) side view of the atomic structure of penta-SiC_2 monolayer (2×2 supercell). d_1 and d_2 are the bond length of Si-C and C-C in this pentagonal structures, respectively. h is the buckling distance. (c) is PBE calculated orbital-projected electronic band structures of monolayer penta-SiC_2 along the represents high-symmetry directions of Brillouin zone (BZ) and density of states (DOS) of penta-SiC_2.

C-C bond with three atomic layers (two C atom layers on the top and bottom, and Si atom layer in the middle). As shown in Table. I, the associated lattice constant of penta-SiC_2 is a=b=4.41 Å with the buckling height h=1.33 Å. The bonding lengths are d_1=1.91 Å and d_2=1.36 Å, which are in good agreement with previously theoretical results[20]. To avoid artificial interaction between atom layers, the separation between the layers is set to be 15 Å for monolayer penta-SiC_2.

The PBE calculations show that, SiC_2 is a semiconductor with an indirect band gap of 1.39 eV, and the minimum of the conduction band (VBM) is located at S point, the maximum of the valence band (VBM) is located between S and Γ points. The corresponding HSE06 calculation gives a larger band gap of 2.85 eV comparing to the PBE result since PBE always underestimates the value of band gap of semiconductors. Fig. 1(c) shows the PBE calculations of orbital-projected electronic band structures and density of states (DOS) of penta-SiC_2. Analysis on the PDOS (Si-3s, 3p and C-2s, 2p orbitals) of penta-SiC_2 reveals that C-2p and Si-3p orbitals mainly dominate the electronic states near the Fermi level. However, the contributions by the C-2p states to the total DOS is larger than that by Si-3p, and in the energy range of -2 to 0 eV for valence band, the Si-3p states contribute larger than that by C-2p, indicating the strong hybridization between the Si 3p states and C 2p states. The analysis on the chemical bonding of pengta-SiC_2 based on the DOS is in consistency with the calculated bond lengths, which show an identical length of Si-C

TABLE I. Calculated structure properties of 2D penta-SiC_2: lattice constant(a, b), buckling distance (h), Si-C and C-C bond length (d_1, d_2). The magnitude of band gap calculated under PBE and HSE06 approximation respectively.

structure	lattice constant[Å]	h[Å]	d_1[Å]	d_2[Å]	$E_g(PBE)[eV]$	$E_g(HSE)[eV]$	Young's modulus(GPa)
penta-SiC_2	4.41	1.33	1.91	1.36	1.39	2.85	292

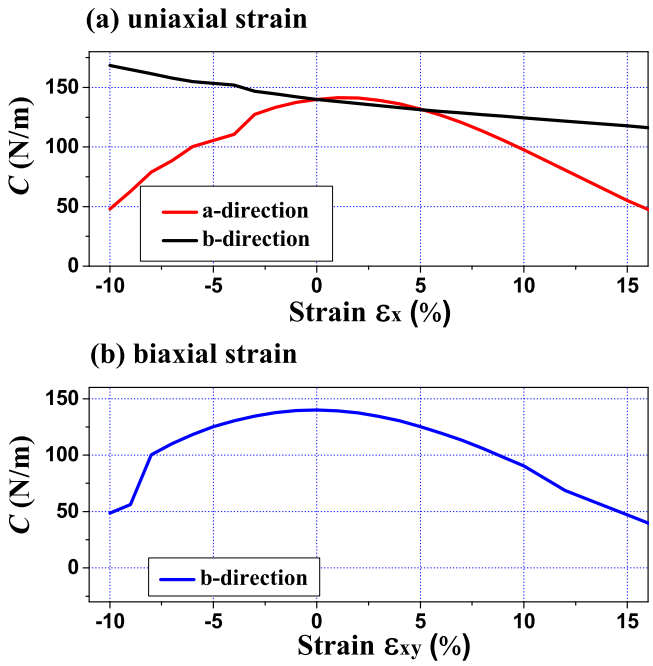

FIG. 2. Calculated elastic modulus C_{ij}^{2D}along a- and b-directions under various mechanical strain for penta-SiC_2.

bonding. The four identical bond lengths and bonding angles indicate that Si atom connects to the four neighboring C atoms via sp^2d hybridization. Similar analysis on C atoms shows that C connects to the two neighboring Si atoms and one C atom via sp^3 hybridization.

B. Strain-engineering mechanical properties of penta-SiC_2

We have studied the effects of in-plane uniaxial and biaxial strains on mechanical, electron and transport properties of penta-SiC_2. Here, ε_x, ε_y and ε_{xy} refer to the components of relative strain along $a-$, $b-$ and bi$(a+b)$-directions respectively. Since penta-SiC_2 has nearly isotropic physical properties along a- and b-directions respectively, only the strain ε_x is considered in the following.

In addition, under the in-plane biaxial strain, the physical properties are nearly the same along a- and b-directions, so only the physical properties along the b-direction are presented here. The positive (negative) signs of strains represent tensile (compressive) strain, and the value of strain is evaluated as the lattice stretching (condensing) percentage.

Due to three-dimensional (3D) periodic boundary conditions, the 2D elastic constant C_{ij}^{2D} should be rescaled by multiplying the c lattice parameter corresponding to the vacuum space between 2D layers[21], *i.e.*, $C_{ij}^{2D} = c\, C_{ij}^{3D}$. The calculated in-plane elastic constant $C_{11}^{2D} = C_{22}^{2D} = 140\ N/m$ for penta-SiC_2, indicates that penta-SiC_2 has nearly isotropic mechanical property. The positive values of C_{11}^{2D} and C_{22}^{2D} mean that penta-SiC_2 is mechanically stable, according to the the mechanical stability criteria. The 3D Young's modulus Y can be expressed as $Y = C_{ij}^{2D}/t$, where t is the effective thickness of penta structure (4.8 Å for penta-SiC_2), and the calculated value of Y is 292 GPa for SiC_2, similar to that of MoS_2 (270 ± 100 GPa)[22], while larger than that of black phosphorene (experimental values: 179 GP and 55 GP along a- and b-directions respectively)[23], TiS_3 (96 GP and 153 GP along a- and b-directions respectively)[14] and HfS_2 (137 GPa)[14]. The difference can be attributed to the bond length and bond density of different 2D materials.

Furthermore, we have calculated the elastic modulus along the a- and b-directions under various mechanical strain, as shown in Fig. 2. By stretching (compressiving) the atom-atom bond length, it is shown that a decreased (increased) of bond energy may reduce (enlarge) the value of elastic constant. Fig. 2(a) shows the dependence of elastic constant along a- and b-directions under uniaxial (ε_x) strain. Under uniaxial strain, the elastic constant decreases monotonously in the range of $-10\% \leq \varepsilon_x \leq 10\%$ along a-direction, while along b-direction, it has a maximum value at a tensile strain of ε_x=1% and decrease linearly from ε_x=1% to 10%, and under compressive strain, the elastic constant decreases linearly at a high rate. While for biaxial strain as shown in Fig. 2(b), the value of elastic modulus of two directions decreases with similar tendency of b-direction under uniaxial strain for penta-SiC_2.

C. Strain-engineering electronic properties of penta-SiC_2

Fig. 3 shows the evolution of the valence and conduction band structures as a function of different strains, mainly from −10% to 10% of the fully relaxed structure. Fig. 3 (a) and (b) show the dependence of the energy bands of monolayer penta-SiC_2 on strain along a- and bi-directions, respectively. The shift of the band edge as shown in Fig. 3 (a) and (b) can be understood in terms

of the bonding and antibonding states[24]. The VBMs (V_s and V_Γ) and the CBMs (C_s and $C_{s-\Gamma}$) are shown in Fig. 3 (a) and (b). The monolayer penta-SiC_2 is an indirect semiconductor described by VBM of V_s and CBM of $C_{s-\Gamma}$. However, by applying an uniaxial tensile strain (ε_x), the energies corresponding to the V_s and $C_{s-\Gamma}$ change greatly, which transforms penta-SiC_2 into a new type of indirect semiconductor formed by VBM of V_Γ and CBM of C_s. Under uniaxial compressive strain, $C_{s-\Gamma}$ decreases while V_s increases, leading to a shrinking indirect band gap of the strained penta-SiC_2. While for an external strain along bi-direction (ε_{xy}), large changes take place for the energies corresponding to V_s, V_Γ, C_s and $C_{s-\Gamma}$ as shown in Fig. 3 (b). When $\varepsilon_{xy} = -8\%$, the semiconductor(indirect)-to-metal transition takes place. The strain tunable electronic structure of monolayer SiC_2 will significantly influence the electronic transport properties, which can be used in the electronic and optoelectronic applications.

Fig. 3 (c) and (d) shows the evolution of calculated band gap under various strains. When applying the in-plane uniaxial strain for $-15\% \leq \varepsilon_x \leq 22\%$, penta-$SiC_2$ remains an indirect semiconductor with a maximum band gap of 1.481 eV at 2%, while the gap energies and the positions of the VBM and CBM change. However, when applying the in-plane biaxial strain for $-15\% \leq \varepsilon_{xy} \leq 15\%$, penta-$SiC_2$ also remains the indirect semiconducting feature, and it converts into a metal beyond 15% and −9%. However, the band gap reaches a maximum value of 1.483 eV at the strain of 1%.

As can be seen in Fig. 3 (c) and (d), the electronic band gap is very sensitive to the application of compressive and tensile strain. The reason may be that penta-SiC_2 exhibits a partial inversion of the vertical ordering of the p-p-σ and p-p-π electronic bands, and the energy states corresponding to the in-plane σ-orbitals are located in the vicinity of the Fermi level. Meanwhile, the in-plane σ-bonds is sensitive to variations in the bonding length, which is the main factor leading to the variation of band gap upon different strains[10].

In order to understand the contribution of different orbitals from different atoms to the electronic states, we have calculated the total (DOS) and partial (PDOS) densities of states for penta-SiC_2 with tensile and compressive strains: ±10% strains along a-direction and bi-direction, respectively, as shown in Fig. 4. By comparison, it's obvious that the contribution from different orbits of Si and C atoms to the valence band does not change too much when uniaxial or biaxial strain is applied. However, when uniaxial or biaxial compressive strain larger than $\varepsilon_x = -10\%$ is applied, the contribution from C $2p$ states becomes dominant. Therefore, when monolayer penta-$SiC_2$is free of strain or under small strain (less than 10%), the conduction band mainly constructs the low

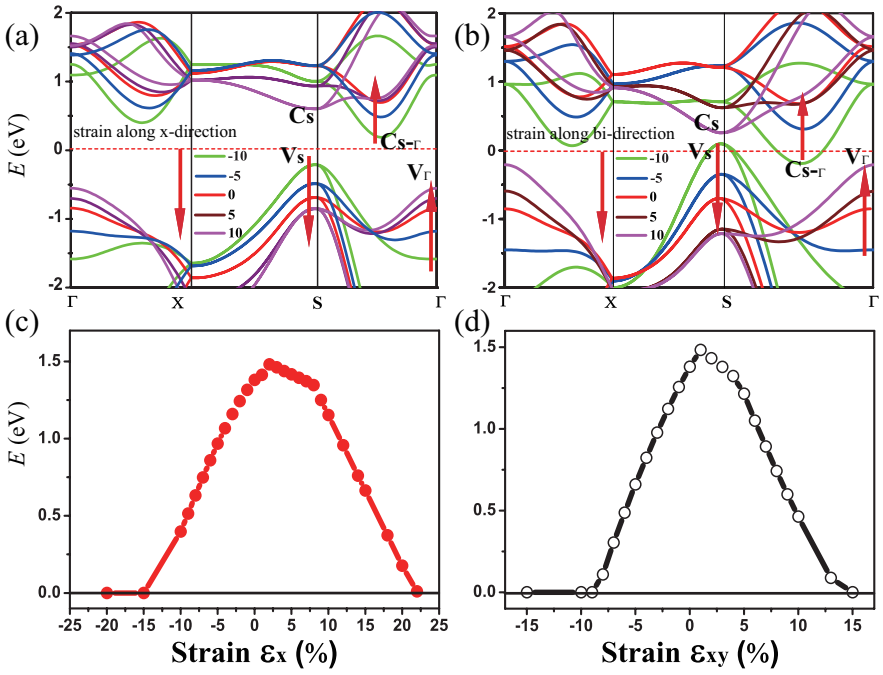

FIG. 3. PBE calculated band structures under (a) uniaxial (a-direction) strain and (b) biaxial (bi-direction) strain for penta-SiC_2. (c) and (d) show the evolution of band gap for SiC_2 as a function of the applied various (uniaxial and biaxial) strain, respectively. Furthermore, the crystal structure is fully relaxed(both unit cell parameters and atomic positions under symmetry constraints).

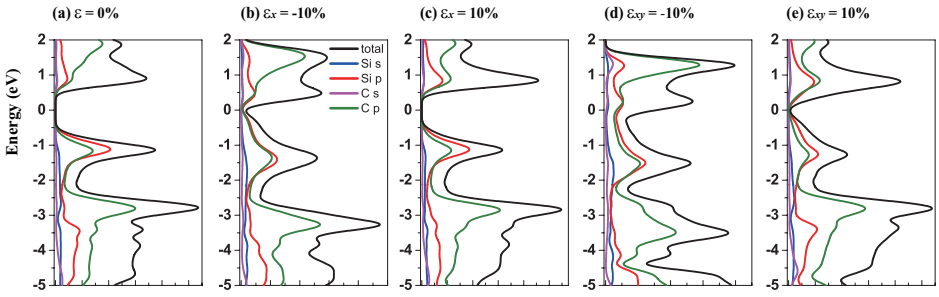

FIG. 4. PBE calculated total and partial densities of states for penta-SiC_2 under uniaxial and biaxial strain with compressive and tensile strength: (a) no strain, (b) $\varepsilon_x = -10\%$, (c) $\varepsilon_x = 10\%$, (d) $\varepsilon_{xy} = -10\%$, and (e) $\varepsilon_{xy} = 10\%$, respectively.

hybridization states of Si $3p$ and C $2p$ orbits, when a large strain is applied, the contribution from C $2p$ states overwhelms that from Si $3p$ states.

D. Strain-engineering transport properties of penta-SiC_2

Here we perform the deformation potential theory, which was proposed by Bardeen and Shockley[25] to analyze the intrinsic carrier mobility u, and has been widely used in low-dimensional systems[15,26–28]. Based on the acoustic phonon limited approach[25], the charge carrier mobility of 2D material can be written as,

$$\mu = \frac{2e\hbar^3 C}{3k_B T|m^*|^2 E_l^2}, \tag{1}$$

where e is the electron charge, T is the temperature which is equal to 300 K throughout the paper. C is the elastic modulus of a uniformly deformed crystal by strains, m^* is the effective mass given by $m^* = \hbar^2(\partial^2 E(k)/\partial k^2)^{-1}$ (where $\hbar$ is the reduced Planck's constant, k is the magnitude of wave-vector in momentum space, and $E(k)$ denotes the energy corresponding to the wave vector). E_l is the DP constant defined by $E_l^{e(h)} = \Delta E_{CBM(VBM)}/(\delta l/l)$, where $\Delta E_{CBM(VBM)}$ is the energy shift of the band edge with respect to the vacuum level under a small dilation δl of the lattice constant l.

According to Eq. (1), the carrier mobility of electrons and holes along certain directions for penta-SiC_2 are obtained, as shown in Fig. 7 and Table. III. Although the PBE calculations always underestimate the band gap, the calculated carrier mobilities are in good agreement with experimental results for many 2D materials[15,26,27,29,30]. Firstly, we compare the a-direction uniaxial strain modulated charge carrier mobility of penta-SiC_2 along a- and b-directions as shown in Fig. 7. Three different physical parameters, namely carrier effective mass (m^*), DP constant (E_l) and elastic modulus (C), are subjected to change at a particular temperature under strain.

The band structures of strained penta-SiC_2 change when the structure changes, which subsequently alter the effective mass of carriers determined by the curvatures of band edges near the Fermi level. Fig. 5 demonstrates the evolution of the calculated effective masses of electrons (m_e^*) and holes (m_h^*) along a- and b-directions under uniaxial strains along a-direction. The m_h^* at S point is $0.29m_0$ and m_e^* at $S-\Gamma$ point is $0.90m_0$ without strain (m_0 is the static electron mass). As shown in Fig. 3(a), applied strains along a-direction ε_x may lead to large shifts of the positions of VBMs and CBMs in the band structures. The VBM of penta-SiC_2 shifts from V_s to V_Γ with the strain of $\varepsilon_x = 3\%$, which results in a dramatic increase of m_h^* ($0.30m_0 \rightarrow 0.69m_0$ along a-direction, and $0.28m_0 \rightarrow 0.74m_0$ along b-direction) when ε_x increases from 2% to 3%. Meanwhile, The CBM of penta-SiC_2 shifts from $C_{s-\Gamma}$ to C_s with the strain of $\varepsilon_x = 8\%$. Therefore a dramatic change of electron effective mass occurs as well when the uniaxial strain changes from $\varepsilon_x = 7\%$ to $\varepsilon_x = 8\%$. The subsequent m_e^* reduces significantly from $1.33m_0$ to $0.33m_0$, and the b-direction m_e^*

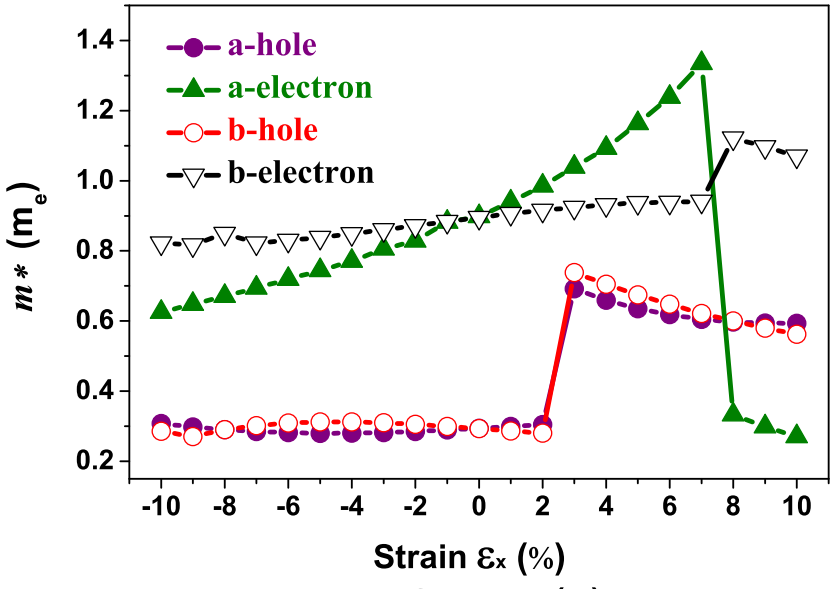

FIG. 5. Respective dependence of calculated carrier (hole m_h^* and electron m_e^*) effective masses along the a- and b-directions on the applied uniaxial strains.

increases from $0.94m_0$ to $1.12m_0$, as shown in Fig. 5. Additionally, the anisotropic effective mass under strains will lead to anisotropic carrier mobilities, which finally lead to direction-dependent electron conductivity.

In order to calculate DP constant, a small dilation need to be applied along the direction. The calculated DP constant for holes is 2.98 eV and 3.00 eV for electrons, respectively, which are in good agreement with previous theoretical results[20]. Fig. 6 demonstrates the evolution of the electron (E_{l-e}) and hole (E_{l-h}) DP constants along a- and b-directions under uniaxial strains along a-direction. Similar to the case of effective masses, the shifts of VBMs with a uniaxial strain of $\varepsilon_x = 3\%$ and CBMs with a strain of $\varepsilon_x = 8\%$ cause dramatic changes of DP constants of holes and electrons, respectively, as shown in Fig. 6. Interestingly, the obtained b- direction E_{l-h} of holes is low ($0.15eV \rightarrow 0.40eV$) in the strain range of $-10\% \leq \varepsilon_x \leq -6\%$, which subsequently results in high hole-carrier mobilities larger than $10^5 cm^2/Vs$ along a particular direction as shown in Fig. 7.

The dependence of calculated carrier mobilities on the uniaxial strain is shown in Fig. 7. The obtained hole and electron mobilities without strain are $2.59\times10^3 cm^2/Vs$ and $2.74\times10^2 cm^2/Vs$, respectively. For uniaxial strain along the a-direction, dramatic enhancement of the hole mobility along the b-direction under compressive strains is observed, increasing from $2.59\times10^3 cm^2/Vs$ to

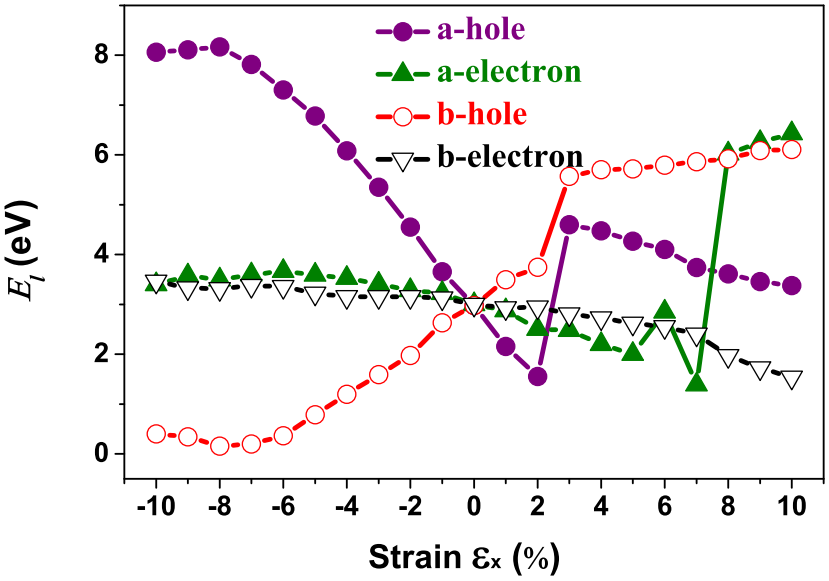

FIG. 6. Calculated carrier (hole and electron) deformation potential constant (E_l) along the a- and b-directions as a function of the applied uniaxial strain.

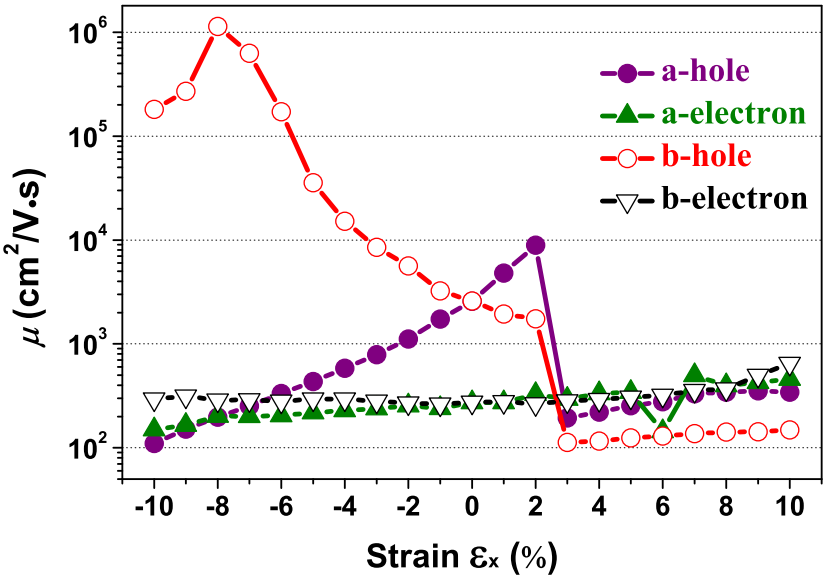

FIG. 7. Calculated charge carrier (hole and electron) mobility (u) along the a- and b-directions as a function of the applied uniaxial strain, respectively.

TABLE II. Calculated carrier mobility of strained pengta-SiC in comparison to those of monolayer graphene, silicene, balck phosphorene and MoS_2. (Unit of carrier mobilities, $cm^2/V \cdot s$.)

carrier mobility	penta-SiC_2	graphene[31]	silicene[31]	balck phosphorene[16,33]	MoS_2[15,32]
hole	1.14×10^6	3.51×10^5	2.23×10^5	286	200
electron	649	3.39×10^5	2.58×10^5	2.2×10^3	72, ~ 200

$1.14 \times 10^6 cm^2/Vs$ at $\varepsilon_x = -8\%$. In Table. II, the calculated carrier mobilities of strained penta-SiC and some widely-investigated two-dimensional semiconductor are listed. By comparison, it is found that, the hole carrier mobility of penta-SiC_2 stained by $\varepsilon_x = -8\%$ is ultrahigh, an order of magnitude larger than those of graphene ($2.58 \times 10^5 cm^2/Vs$)[31], silicene ($3.39 \times 10^5 cm^2/Vs$)[31], three or four orders higher than those of monolayer black phosphorene ($2.2 \times 10^3 cm^2/Vs$)[16], MoS_2($\sim 200 cm^2/Vs$)[15,32], which indicates that strain-engineering monolayer pent-SiC_2 can be quite promising for the application of microelectronics.

Meanwhile, strain-engineering has little influence on the electron mobility along both a- and b-directions, as shown in Fig. 7. The hole mobility along the a-direction increases nearly linearly from $2.59 \times 10^3 cm^2/Vs$ to $1.0 \times 10^4 cm^2/Vs$ in the strain range of $\varepsilon_x = -10\%$ to 2%, which can be attributed to the monotonic decrease of effective masses of holes along a-direction, according to Eq. (1).

Table. III shows the evolution of the effective mass (m_b^*), DP constant (E_{l-b}), elastic modulus (C_b) and the calculated results of hole and electron mobilities along b-direction under biaxial strains. For the hole mobility as listed in Table. III, since all the three decisive parameters (m_b^*, E_{l-b} and C_b) increase by applying tensile and compressive strain, the hole mobilities for strained structures are thus smaller than that without strain according to Eq. (1). The obtained electron mobility increases monotonically from $\varepsilon_{xy} = -10\%$ to $\varepsilon_{xy} = 10\%$, mainly caused by the decrease of the effective mass m_e^*.

IV. CONCLUSION

To summarize, we have demonstrated the evolution of structure, electronic and charge carrier transport properties of penta-SiC_2 under uniaxial or biaxial strain. Based on the first-principles calculation using the PBE functional method, SiC_2 is found to be a semiconductor with a direct band gap of 1.39 eV, and HSE06 functional gives the band gap of 2.85 eV. By employing Voigt

TABLE III. The effective mass and charge carrier mobilities in penta-SiC_2, It shows the calculated effective mass m_b^* (with m_0^* being the static electron mass), deformation potential constant E_{l-b}, 2D elastic modulus C_b along the $\Gamma - Y$ direction, The electron and hole carrier mobility (μ_b) are calculated by using Eq.(1) at T=300 K.

Carrier type	ε_{xy} [%]	m_b^* [m_0]	E_{l-b} [eV]	C_b [N/m]	μ_b [$\times 10^2 cm^2/V \cdot s$]	Carrier type	ε_{xy} [%]	m_b^* [m_0]	E_{l-b} [eV]	C_b [N/m]	μ_b [$\times 10^2 cm^2/V \cdot s$]
hole	-10	0	0	0	0	electron	-10	0	0	0	0
	-8	0.29	5.45	100.37	5.78		-8	0.67	3.66	100.37	2.24
	-6	0.30	4.78	118.29	8.43		-6	0.71	3.55	118.29	2.60
	-4	0.30	4.12	130.41	12.31		-4	0.75	3.47	130.41	2.72
	-2	0.30	4.03	137.66	13.68		-2	0.80	3.31	137.66	2.76
	0	0.29	2.99	139.89	25.88		0	0.90	3.0	139.89	2.74
	2	0.66	5.29	137.31	1.58		2	1.05	2.61	137.31	2.60
	4	0.55	4.80	130.34	2.65		4	1.30	1.81	130.34	3.30
	6	0.48	4.34	119.47	3.91		6	0.52	4.13	119.47	3.62
	8	0.43	4.00	106.01	4.99		8	0.46	3.96	106.01	4.44
	10	0.40	3.62	90.39	6.03		10	0.43	3.68	90.39	5.14

notation, penta-SiC_2 has a relatively high Young's modulus: 292 GPa. The transition point from semiconductor to metal is different between uniaxial and biaxial strains. The hole mobility along b-direction can be significantly improved by a-direction compressive strain. Meanwhile, strain-engineering has relatively little effect on electron mobility. Therefore, it would be helpful to select carrier type based on their different transport properties under various strains. This study gives us a comprehensive understanding of the strain effect on the electronic properties of monolayer penta-SiC_2, and the properties may find applications in nanoscale strain tensor and conductance-switch field effect transistor storages.

ACKNOWLEDGEMENT

This work is supported by the National Natural Science Foundation of China under Grants No. 11374063 and 11404348, and the National Basic Research Program of China (973 Program) under

Grants No. 2013CBA01505.

---

[1] K. S. Novoselov, A. K. Geim, S. V. Morozov, D. Jiang, Y. Zhang, S. V. Dubonos, I. V. Grigorieva, and A. A. Firsov. Electric field effect in atomically thin carbon films. *Science*, 306(5696):666–669, 2004.

[2] K. S. Novoselov, A. K. Geim, S. V. Morozov, D. Jiang, Katsnelson M. I., I. V. Grigorieva, and A. A. Dubonos, S. V.and Firsov. Two-dimensional gas of massless dirac fermions in graphene. *Nature*, 438:197–200, 2005.

[3] Horst L. Stormer Yuanbo Zhang, Yan-Wen Tan and Philip Kim. Experimental observation of the quantum hall effect and berry's phase in graphene. *Nature*, 438, 2005.

[4] Alexander A. alandin. Thermal properties of graphene and nanostructured carbon materials. *Nat. Mater.*, 10:569–581, 2011.

[5] Alexander A. Balandin, Suchismita Ghosh, Wenzhong Bao, Irene Calizo, Desalegne Teweldebrhan, Feng Miao, and Chun Ning Lau. Superior thermal conductivity of single-layer graphene. *Nano Letters*, 8:902–907, 2008.

[6] F. Schedin, A. K. Geim, S. V. Morozov, E. W. Hill, P. Blake, M. I. Katsnelson, and K. S. Novoselov. Detection of individual gas molecules adsorbed on graphene. *Nat. Mater.*, 6:652–655, 2007.

[7] Shunhong Zhang, Jian Zhou, Qian Wang, Xiaoshuang Chen, Yoshiyuki Kawazoe, and Puru Jena. Penta-graphene: A new carbon allotrope. *Proc. Natl. Acad. Sci.*, 112(8):2372–2377, 2015.

[8] Wen Xu, Gang Zhang, and Baowen Li. Thermal conductivity of penta-graphene from molecular dynamics study. *J. Chem. Phys.*, 143(15), 2015.

[9] Yierpan Aierken, Ortwin Leenaerts, and Franois M. Peeters. A first-principles study of stable few-layer penta-silicene. *Phys.Chem.Chem.Phys.*, 18:18486–18492, 2016.

[10] Alejandro Lopez-Bezanilla and Peter B. Littlewood. $\sigma\pi$-band inversion in a novel two-dimensional material. *The Journal of Physical Chemistry C*, 119(33):19469–19474, 2015.

[11] Ji Feng, Xiaofeng Qian, Cheng Wei Huang, and Ju Li. Strain-engineered artificial atom as a broad-spectrum solar energy funnel. *Nat. Photon.*, 6:866–872, 2012.

[12] Hiram J. Conley, Bin Wang, Jed I. Ziegler, Jr. Richard F. Haglund, Sokrates T. Pantelides, , and Kirill I. Bolotin. Bandgap engineering of strained monolayer and bilayer mos_2. *Nano Lett.*, 13:3626–3630, 2013.

[13] Sheng Yu, Hao Zhu, Kwesi Eshun, Chen Shi, Min Zeng, and Qiliang Li. Strain-engineering the anisotropic electrical conductance in res_2 monolayer. *Appl. Phys. Lett.*, 108:191901, 2016.

[14] Jun Kang, Hasan Sahin, and Franois M. Peeters. Mechanical properties of monolayer sulphides: a comparative study between mos_2, hfs_2 and tis_3. *Phys.Chem.Chem.Phys.*, 17:27742–27749, 2015.

[15] Y. Cai, G. Zhang, and Y.W Zhang. Polarity-reversed robust carrier mobility in monolayer mos_2 nanoribbons. *J. Am. Chem. Soc.*, 136:62696275, 2014.

[16] Ruixiang Fei and Li Yang. Strain-engineering the anisotropic electrical conductance of few-layer black phosphorus. *Nano Lett.*, 14(5):28842889, 2014.

[17] Deniz akr Yierpan Aierken and Francois M. Peeters. Strain enhancement of acoustic phonon limited mobility in monolayer tis_3. *Phys.Chem.Chem.Phys.*, 18:14434–14441, 2016.

[18] G. Kresse and J. Furthmüller. Efficient iterative schemes for *ab initio* total-energy calculations using a plane-wave basis set. *Phys. Rev. B*, 54:11169–11186, 1996.

[19] Jochen Heyd, Gustavo E. Scuseria, and Matthias Ernzerhof. Hybrid functionals based on a screened coulomb potential. *The Journal of Chemical Physics*, 118(18):8207–8215, 2003.

[20] Xinru Li, Ying Dai, Mengmeng Li, Wei Wei, and Baibiao Huang. Stable si-based pentagonal monolayers: high carrier mobilities and applications in photocatalytic water splitting. *J. Mater. Chem. A*, 3:24055–24063, 2015.

[21] Michael N. Blonsky, Houlong L. Zhuang, Arunima K. Singh, and Richard G. Hennig. Ab initio prediction of piezoelectricity in two-dimensional materials. *ACS Nano.*, 9(10):98859891, 2015.

[22] Simone Bertolazzi, Jacopo Brivio, and Andras Kis. Stretching and breaking of ultrathin mos_2. *ACS Nano.*, 5(12):97039709, 2011.

[23] Qun Wei and Xihong Peng. Superior mechanical flexibility of phosphorene and few-layer black phosphorus. *Appl. Phys. Lett.*, 104(25):251915, 2014.

[24] C. Kamal and Motohiko Ezawa. Arsenene: Two-dimensional buckled and puckered honeycomb arsenic systems. *Phys. Rev. B*, 91:085423, 2015.

[25] J. Bardeen and W. Shockley. Deformation potentials and mobilities in non-polar crystals. *Phys. Rev.*, 80:72–80, Oct 1950.

[26] Mengqiu Long, Ling Tang, Dong Wang, Yuliang Li, and Zhigang Shuai. Electronic structure and carrier mobility in graphdiyne sheet and nanoribbons: Theoretical predictions. *ACS Nano.*, 5(4):25932600, 2011.

[27] J. Chen, J. Xi, D. Wang, and Z Shuai. Carrier mobility in graphyne should be even larger than that in graphene: A theoretical prediction. *J. Phys. Chem. Lett.*, 4:14431448, 2013.

[28] Yanli Wang and Yi Ding. Electronic structure and carrier mobilities of arsenene and antimonene nanoribbons:a first-principle study. *Nanoscale Res. Lett.*, 10:254, 2015.

[29] Jun Dai and Xiao Cheng Zeng. Titanium trisulfide monolayer: Theoretical prediction of a new direct-gap semiconductor with high and anisotropic carrier mobility. *Angew. Chem.*, 127:7682 7686, 2015.

[30] Jinyang Xi, Mengqiu Long, Ling Tang, Dong Wang, and Zhigang Shuai. First-principles prediction of charge mobility in carbon and organic nanomaterials. *Nanoscale*, 4:4348–4369, 2012.

[31] Zhi-Gang Shao, Xue-Sheng Ye, Lei Yang, and Cang-Long Wang. First-principles calculation of intrinsic carrier mobility of silicene. *J. Appl. Phys.*, 114:093712, 2013.

[32] Sunkook Kim, Aniruddha Konar, Wan sik Hwang, Jong Hak Lee, Jiyoul Lee, Jaehyun Yang, and Changhoon Jung et al. High-mobility and low-power thin-film transistors based on multilayer mos2 crystals. *Nat. Commun.*, 3(1011), 2012.

[33] Jun Liu, Gyung-Min Choi, and David G. Cahill. Measurement of the anisotropic thermal conductivity of molybdenum disulfide by the time-resolved magneto-optic kerr effect. *Journal of Applied Physics*, 116(23):233107, 2014.